Chain-Folding and Overall Molecular Conformation in a Novel Amphiphilic Starlike Macromolecule

Jianjun Miao,[†] Guoqiang Xu,[‡] Lei Zhu,[*,†] Lu Tian,[§] Kathryn E. Uhrich,[§] Carlos A. Avila-Orta,[⊥] Benjamin S. Hsiao,[⊥] and Marcel Utz[#]

Polymer Program, Institute of Materials Science and Department of Chemical Engineering, The University of Connecticut, Storrs, Connecticut 06269-3136; Baker Laboratory of Chemistry and Chemical Biology, Cornell University, Ithaca, New York 14853; Department of Chemistry and Chemical Biology, Rutgers University, Piscataway, New Jersey 08854; Chemistry Department, State University of New York at Stony Brook, Stony Brook, New York 11794; and Polymer Program, Institute of Materials Science and Department of Physics, The University of Connecticut, Storrs, Connecticut 06269

Received May 11, 2005; Revised Manuscript Received June 5, 2005

ABSTRACT: The crystallization and self-assembly behavior of an amphiphilic starlike macromolecule (ASM) with a lipophilic core and four poly(ethylene oxide) (PEO) arms (M_n = 2000 g/mol) were characterized by synchrotron small-angle X-ray scattering (SAXS) and wide-angle X-ray diffraction at different crystallization temperatures (T_c). The overall d-spacing of the alternating amorphous core and crystalline PEO lamellae almost doubled from 11.4 nm for samples quenched into liquid nitrogen to 21.0 nm for T_c = 42 °C, indicating gradual transitions from nearly once-folded to fractionally folded and finally to extended chain crystals with increasing the T_c. On the basis of SAXS, transmission electron microscopy, and computer simulation results, it was suggested that the lamellae contained an interdigitated, single-layered PEO crystal, and an amorphous layer consisted of a double-layered lipophilic core and amorphous PEO. A folded (four PEO arms at one side of the core) rather than an extended (two PEO arms on each side of the core) overall molecular conformation (OMC) of the ASM was deduced in the solid state. These results implied that chain-folding and OMC of the ASM closely depended on its star-block-like architecture.

Introduction

Self-assembly of amphiphilic molecules depends on intermolecular interactions, molecular architecture, and the relative ratio between lipophilic and hydrophilic moieties.[1] For example, if one moiety has a high tendency to crystallize, self-assembly of the amphiphilic molecule must consider the crystallization process.[2,3] Polymer crystallization is a special self-assembly process with unique characteristics; it is known that chain-folded crystalline lamellae are basic morphological building blocks of larger structures such as spherulites.[4] Unlike chain-folding in proteins, which represents the thermodynamic equilibrium,[5] polymer chain-folding is kinetically driven and thus necessary for the formation of lamellar morphology.[6] Monodisperse oligomers show a unique chain conformation in the solid state, namely, integral folding[7,8] where the number of folds depends on the molecular weight. For example, short oligomers can only form extended chain crystals; the chain ends are rejected from the crystalline region to both basal planes in order to minimize the overall free energy.[6] Nevertheless, nonintegral folding (including fractional folding) has been observed as a kinetically favorable process in oligomer crystallization.[9,10] The nonintegrally folded crystals can transform into integrally folded crystals through a thinning and/or thickening process.[6]

If multiple components are introduced into well-defined crystalline oligomers, interactions between the different components lead to hierarchical self-assembly to form secondary and even tertiary structures.[11] The resulting phase structures can be manipulated through the microphase segregation between chemically distinctive constituents, such as highly immiscible polyethylene (PE) and poly(ethylene oxide) (PEO).[12]

For semicrystalline diblock copolymers of uniform chain length, chain-folding is predicted under equilibrium conditions, rather than a kinetically controlled process, due to a free energy balance between chain-folding of the crystalline block and chain-stretching of the amorphous block.[13−15] As a consequence, the thickness (d) of the crystalline domains should be uniform and scale as $d \sim N_t N_a^a$, where N_t and N_a are the degrees of polymerization of the entire diblock and the amorphous block, respectively. Here, a is a constant, e.g., −1/3 reported in ref 13, −5/12 in ref 14, and −6/11 in ref 15. Experimental studies have been carried out to study the equilibrium chain-folding in relatively high molecular weight block copolymers,[16−20] and the results reasonably agreed with the theoretical predictions. However, direct measurements of the crystalline layer thickness were difficult in these experiments. Explicit chain-folding information on number of folds, integral vs nonintegral folds, and chain-end location in nonintegrally folded crystals, therefore, still needed further understanding.

In the cases of oligomeric block copolymers, equilibrium integral chain-folding started at a lower molecular weight threshold, as compared with the oligomeric homologues.[21−27] This was a direct result of the difference in cross-sectional areas of the two blocks at the interface coupled with the need of filling spaces at approximately normal density. For example, an extensive study of the chain-folding in PEO-*block*-poly(butylene oxide) (PEO-*b*-PBO) diblock oligomers, which

[†] Institute of Materials Science and Department of Chemical Engineering, The University of Connecticut.
[‡] Cornell University.
[§] Rutgers University.
[⊥] State University of New York at Stony Brook.
[#] Institute of Materials Science and Department of Physics, The University of Connecticut.
* Corresponding author: e-mail lei.zhu@uconn.edu; Tel 860-486-8708.

10.1021/ma050983q CCC: $30.25
Published on Web 07/09/2005

Scheme 1. Chemical Structure of the ASM

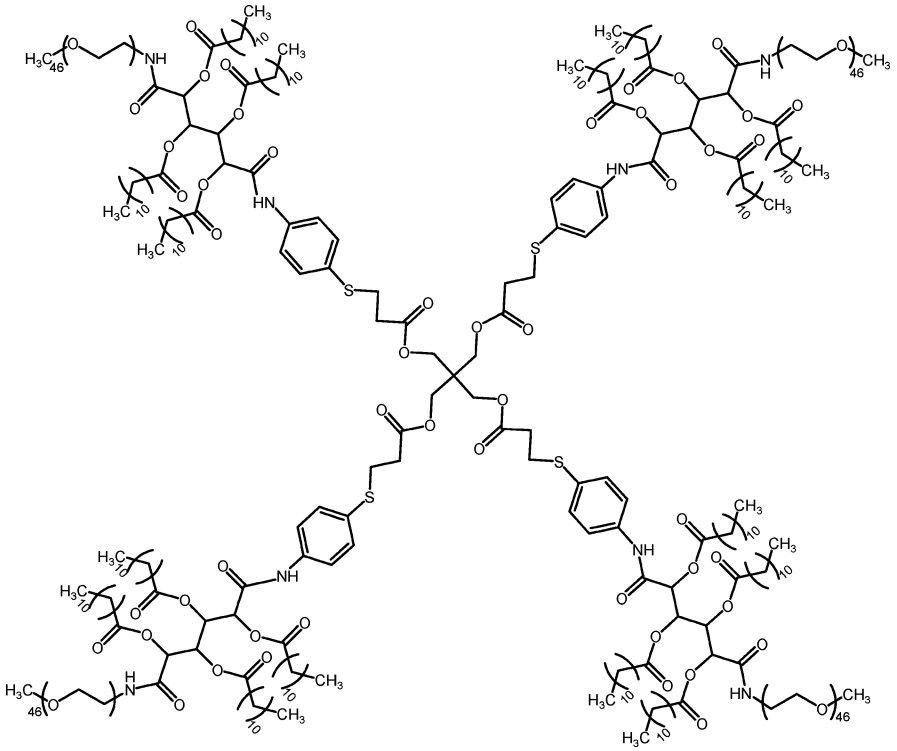

had both disordered and ordered (lamellae, cylinders, and double gyroid) phases in the melt, was carried out using small-angle X-ray scattering (SAXS), wide-angle X-ray diffraction (WAXD), differential scanning calorimetry (DSC), and low-frequency Raman spectroscopy techniques.[26] The crystallinity of these samples ranged from 70 to 83 wt %. In most cases, integral chain-folding was inferred. With increasing the PBO block length, transitions between consecutive fold numbers took place at a lower molecular weight threshold than those in the PEO homooligomers. In these samples, rapid crystallization resulted in metastable multiple-folded (including nonintegrally) structures,[25] and these lamellae could be thickened by annealing at higher temperatures.[26] Similar nonintegral chain-folding was also observed in other PEO-containing block copolymers.[27,28] However, the transformation from the metastable multiple-folded crystals (with more folds) to the equilibrium folded crystals (with fewer folds) was not studied in detail.

When the molecular architecture of oligomers changed from linear to starlike, the overall molecular conformation (OMC) also played an important role in crystallization. For example, two types of OMC were observed for three two-arm PEO samples (number-average molecular weight of each arm being 2200 g/mol), where two linear PEO arms were linked to a phenyl ring at *para*-, *meta*-, and *ortho*-positions, respectively.[29,30] One was an extended OMC with one layer of phenyl defects between two neighboring PEO lamellae (i.e., one PEO arm on each side of a benzene ring), and the other was an once-folded OMC with two layers of phenyl defects between neighboring PEO lamellae (i.e., two PEO arms at the same side of a phenyl ring). In both OMCs in these samples, only extended chain crystals were observed. The relative population of these two OMCs depended not only on crystallization conditions but also on the chemical linkage at the phenyl ring. For example, the sample with an *ortho*-linkage showed exclusively once-folded OMC, while samples with *para*- and *meta*-linkages had mixed extended and once-folded OMCs. The crystals with extended OMC had a slightly lower thermodynamic stability than those with once-folded OMC.

Branched oligomers with three- and four-arm PEOs were also investigated.[31,32] Different from two-arm PEO samples coupled with aryl groups such as 2,4-toluene diisocyanate,[33] extended chain crystals in star PEOs linked with various alcohols (ethylene glycol, glycerol, and pentaerythritol) exhibited higher melting points than the linear precursors.[31] By modifying the model of Flory and Vrij,[34] higher melting point in linked PEOs was interpreted as a result of increased interfacial free energy (σ_e) as the branch number changed. For three- and four-arm PEOs linked by phenyl groups,[32] regular OMC was inferred at low undercoolings. This OMC consisted of extended PEO arms in the crystals and two amorphous layers of the coupling agents and an uncrystallized PEO arm. At high undercoolings, only irregular OMC was observed, and detailed OMC was not reported.

In this work, we have investigated both chain-folding and OMC in a novel amphiphilic starlike macromolecule (ASM) with a lipophilic core and four hydrophilic PEO arms (Scheme 1), which is similar to conventional star-block copolymers. The molecular weight of the core was 4530 g/mol, and each PEO arm was 2000 g/mol. The crystallization behavior of the ASM was studied by simultaneous SAXS and WAXD, DSC, transmission electron microscopy (TEM), and polarized light microscopy (PLM). A lamellar morphology with orthogonal chain orientation in the crystalline lamellae was confirmed by two-dimensional (2D) SAXS and WAXD and TEM. In the isothermal crystallization experiments studied by SAXS, a continuous d-spacing increase from 12.1 nm at the crystallization temperature (T_c) = −20 °C to 21.0 nm at T_c = 42 °C, suggesting that a transition from once-folded to extended crystals occurred via

crystals with fractional folds. Our observations showed that once-folded and fractionally folded crystals were formed kinetically, while extended chain crystals were the equilibrium structure for the ASM sample. In isothermal crystallization experiments, the equilibrium extended chain crystals could only be achieved at an extremely slow rate under a low undercooling. However, annealing of chain-folded crystals (formed at high undercoolings) at elevated temperatures resulted in a fast thickening process to almost extended chain crystals. On the basis of a calculation of the long axis of the cores along the stretching direction, a folded (four arms at the same side of the core) rather than an extended OMC (two neighboring arms on each side of the core) for the ASM was deduced.

Experimental Section

Materials. The ASM in Scheme 1 was synthesized similar to a previously published procedure.[35,36] In brief, the four branches of pentaerythritol tetraacrylate were extended by the Michael addition of 4-aminothiophenol. The hydrophobic core was then prepared by coupling lauroyl derivatives of mucic acid onto the pentaerythritol derivatives. The final polymer was prepared by coupling methoxy-PEO-amine [M_n = 2000 g/mol and polydispersity index (PDI) 1.05] onto the hydrophobic core molecule (M_n = 4530 g/mol). The molecular weight and PDI of the final ASM were 12 530 g/mol and 1.20, respectively, as determined by size exclusion chromatography using polystyrene as standards. Note that ca. 3 wt % PEO homopolymer contamination in the final ASM could result in an increase of the PDI to 1.20. Detailed synthesis and characterization will be published elsewhere.[37]

Characterization and Instrumentation. Simultaneous SAXS and WAXD experiments were performed at the synchrotron X-ray beamlines X3A2 (2D X-ray experiments, wavelength λ = 0.154 nm) and X27C [one-dimensional (1D) X-ray experiments, λ = 0.13 nm] in the National Synchrotron Light Source, Brookhaven National Laboratory. The beam center was calibrated using silver behenate with the primary reflection peak at q = 1.076 nm^{-1}, where the scattering vector $q = 4\pi \sin(\theta/\lambda)$ (θ is the half-scattering angle and λ is the wavelength). The higher-order reflection peaks (up to 11th order) were used for the WAXD calibration. Fuji imaging plates (Fujifilm Medical Systems) were used as 2D detectors. The 2D images were obtained using a Fuji BAS-2500 scanner. Time-resolved 1D SAXS and WAXD were recorded with two European Molecular Biology Laboratory (EMBL) position-sensitive detectors. Temperature-dependent X-ray experiments were performed using an Instec HCS410 hot stage (Instec, Inc.) equipped with a liquid-nitrogen cooling accessory. The azimuthal scans were performed counterclockwise on 2D SAXS and WAXD patterns with the zero-angle starting from the equator, using Polar software (Stony Brook Technology and Applied Research, Inc.). The standard deviation in the peak position was ca. ±3°.

PLM experiments were performed using an Olympus BX51P microscope, also equipped with an Instec HCS410 hot-stage. ASM samples (~1 mg) were sandwiched between thin glass slides and melted at 70 °C for 3 min before subsequent isothermal crystallization at 25 °C. A 1/4-wave lens was used together with cross-polarizers.

TEM experiments were performed on a Philips EM300 at an accelerating voltage of 80 kV. The ASM sample was embedded in standard epoxy before microtoming. Thin sections with a thickness of ~75−100 nm were obtained using a Leica Ultracut UCT microtome with a diamond knife at −50 °C. The thin sections were collected onto 400 mesh TEM grids, freeze-dried, and stained in RuO_4 vapor at room temperature for 10 min.[38]

DSC experiments were carried out on a TA-2920 DSC instrument to study the isothermal crystallization and melting behaviors of the ASM samples. The scanning rate was 5 °C/min for nonisothermal crystallization and melting studies. Less than 1 mg samples were used for the DSC study to avoid thermal lag. After the sample was melted at 70 °C on another hot-plate for 2 min, isothermal crystallization for the PEO blocks was conducted by quenching (hand-transfer) the samples to a preset crystallization temperature (T_c) for a specific time period (~10 times the exothermic peak time). The fully crystallized samples were then heated to 60 °C at a rate of 5 °C/min. The endothermic peak temperature was taken as the melting temperature (T_m).

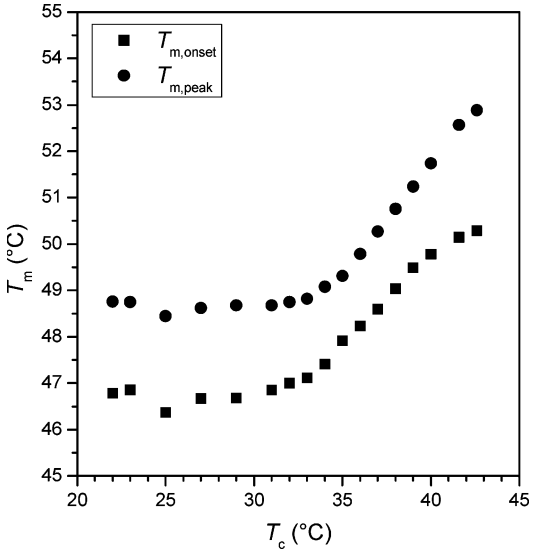

Figure 1. Onset and peak T_ms for the ASM samples crystallized at different T_cs.

Results and Discussion

Crystal Melting Behavior Studied by DSC. Both DSC and WAXD results indicated that only the PEO arms were crystalline with a monoclinic crystalline structure.[4] The DSC melting behavior after isothermal crystallization at various T_cs is summarized in Figure 1. Both the peak ($T_{m,peak}$) and onset ($T_{m,onset}$) melting temperatures remained at 48.5 °C and 46.5 °C, respectively, when the T_c was below 30 °C. Above 30 °C, the peak and onset melting temperatures increased almost linearly with increasing the T_c. The maximum $T_{m,peak}$ value was 52.5 °C for T_c = 42.0 °C, which was close to the equilibrium melting point (ca. 54 °C) for the PEO homopolymer with a molecular weight of 2000 g/mol.[39] The nearly 4 deg increase in the $T_{m,peak}$ clearly indicated different levels of metastability in the PEO crystals at different T_cs. The $T_{m,peak}$ around 48.5 °C for T_c less than 30 °C was resulted from annealed (or reorganized) PEO crystals during a slow heating (5 °C/min). This was proved by simultaneous 1D SAXS and WAXD experiments discussed later. For T_c > 30 °C, the metastability of PEO crystals might be high enough that the true T_ms could be reflected by a 5 °C/min heating rate. To obtain the true T_m values for the PEO crystals formed at low T_cs, fast scan DSC will be used for the future study.

The PEO crystallinity was obtained from the normalized heat of fusion (ca. 90 J/g/64 wt % = 141 J/g) measured in the DSC experiments. For monodisperse PEO homopolymers with a molecular weight of 2000 g/mol, the heat of fusion of extended chain crystals was estimated to be 176.6 J/g.[40] Thus, PEO crystallinity was ca. 80 wt % for fully crystallized ASM samples.

Morphology and Crystal Orientation. The crystalline morphology of the ASM samples on a macro-

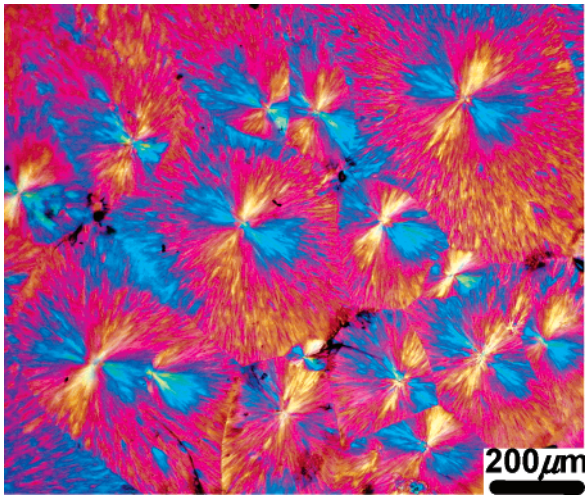

Figure 2. PLM micrograph showing negative birefringent spherulites under a 1/4-wave lens for the ASM sample isothermally crystallized at 25 °C.

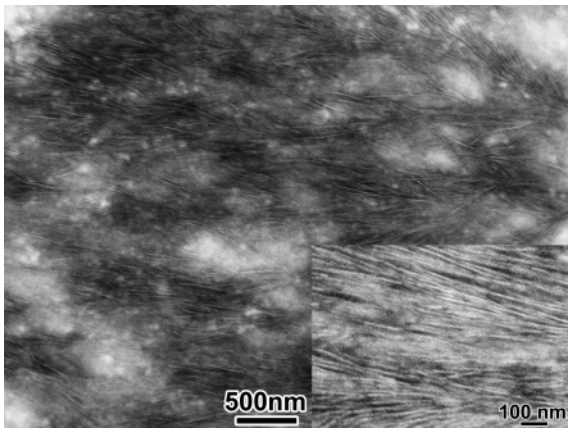

Figure 3. Bright-field TEM micrographs of a thin section ASM sample stained by RuO_4. The inset shows a higher magnification image.

scopic scale was revealed by PLM; a typical micrograph showing negatively birefringent spherulites is shown in Figure 2. The morphology at a microscopic scale was studied by TEM; a typical bright-field micrograph is shown in Figure 3. From the inset, a lamellar structure with alternating bright and dark layers is clearly seen. Judging from the branched lamellar morphology (white lines) in Figure 3, we determined that PEO crystalline lamellae appeared bright, while amorphous cores and PEO were represented by the dark layers. This assignment will be further discussed later.

PEO crystal orientation was studied by simultaneous 2D SAXS and WAXD experiments, as shown in Figure 4. As the ASM sample was isothermally crystallized at 35.0 °C, the 2D SAXS pattern in Figure 4A showed oriented lamellar reflections on the meridian having a q ratio of approximately 1:2, indicating that the crystalline lamellae were stacked horizontally. We noticed that the sample automatically oriented near an air bubble in a thin capillary (diameter = 0.7 mm) during a relatively slow crystallization process. The lamellar orientation was roughly parallel to the bubble surface. The 2D WAXD pattern in Figure 4B showed two oriented reflection rings. The inner ring is the (120) reflection, and the outer ring included mixed reflections such as ($\bar{1}32$), (032), ($\bar{2}12$), (112), etc.[41] This pattern was similar to the PEO fiber pattern reported before.[42] The

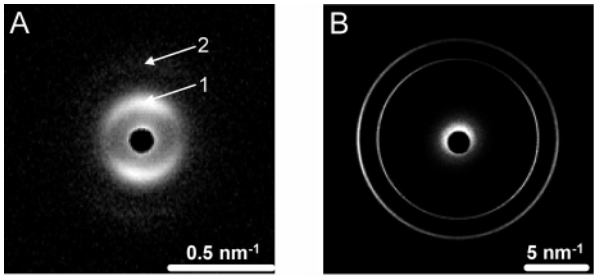

Figure 4. Simultaneous 2D (A) SAXS and (B) WAXD of the ASM isothermally crystallized at 35.0 °C. The intensities in both patterns are in logarithmic scales. The first- and second-order reflections are indicated by the arrows.

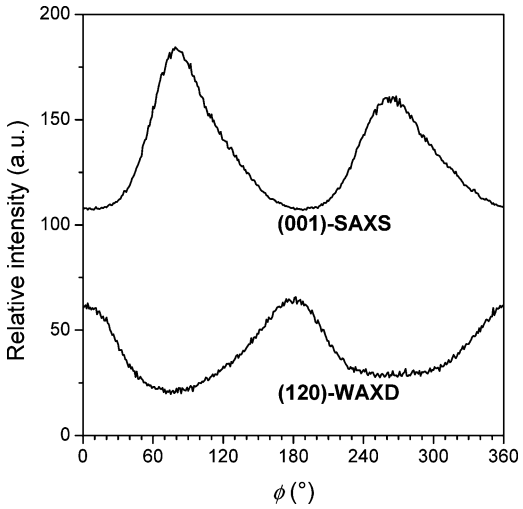

Figure 5. Azimuthal scan results for the lamellar (001) reflection in the SAXS and the PEO (120) reflection in the WAXD in Figure 4. Curves are offset for clarity.

azimuthal scan results of the lamellar (001) reflection in the SAXS and the PEO (120) reflection in the WAXD are shown in Figure 5. The maxima of the PEO (120) reflection were at 0° and 180°, suggesting that the c-axes of the PEO crystals were vertically oriented, while the lamellar (001) reflection had maximum intensities at 83° and 275° (on the meridian). The full width at half-maximum of the azimuthal scan profiles was similar for the lamellar (001) and PEO (120) reflections (ca. 60−70°), indicating a similar degree of orientation at different length scales. On the basis of the above results, we concluded that the crystalline PEO chains were parallel to the crystalline lamellar normal.

***T_c*-Dependent Lamellar Thicknesses and Chain-Folding.** On the basis of the molecular weight and the estimated density (ca. 1.0 g/cm^3) of the hydrophobic core, its diameter was calculated to be ca. 2.4 nm, and it occupied a volume of 7.525 nm^3. The average core diameter of 2.4 nm was proved by SAXS experiments shown later. Since the core had a spherical shape, its basal area was 4.6 nm^2, which could accommodate almost 21 crystalline PEO chains (0.214 nm^2 per PEO chain in the solid state[40,42]). Similar to crystalline block oligomers, the PEO arms must fold to compensate for the different cross-sectional areas at the interface. The equilibrium chain-folding (including extended chain conformation) would be determined by a free energy balance from PEO chain-folding and core-stretching.

To quantify both PEO chain-folding and core-stretching, a SAXS study was carried out to investigate the ASM samples isothermally crystallized at different T_cs,

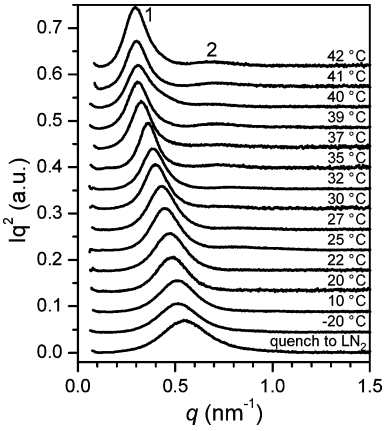

Figure 6. Lorentz-corrected SAXS profiles for the ASM crystallized at different T_cs.

and the results are shown in Figure 6. At low q values, lamellar morphology indicated by the first- and second-order reflections was clearly seen. These SAXS peaks were relatively broad with a full width at half-maximum of 0.2−0.3 nm^{-1}. This could be explained by the fact that the lamellar stacking in the TEM micrograph (Figure 3) was not long-range ordered. With increasing the T_c, the lamellar reflection shifted to lower q values, indicating an increase in the overall lamellar thickness (L). Note that the PEO oligomer with a molecular weight of 2000 g/mol only grew extended chain crystals with a constant thickness of 12.6 nm.[39] The increase in L by a factor of almost 2 was significant, e.g., from L = 11.4 nm for samples quenched into liquid nitrogen (LN_2) to L = 21.0 nm at T_c = 42 °C.

On the basis of these results, we inferred that at low T_cs the PEO chains had to fold, while at high T_cs, more or less extended chain crystals were formed. This is consistent with the observations in crystalline block oligomers;[25−28] at low T_cs kinetically controlled chain-folding had more folds than the equilibrium chain-folding. However, because of a more complicated molecular architecture of the ASM than linear block oligomers, detailed molecular conformation in the solid state needed investigation.

Overall Molecular Conformation of the ASM. Since no obviously overlapped peaks in the range of 0.3−0.8 nm^{-1} were observed in Figure 6, only one population of chain conformation existed in the PEO crystals. Four possible models were proposed for the lamellar morphology in the ASM, namely, (A) a single-layered (interdigitated) crystalline PEO lamella with single-layered cores in an amorphous PEO layer, (B) a double-layered crystalline PEO lamella with single-layered cores in an amorphous PEO layer, (C) a single-layered (interdigitated) crystalline PEO lamella with double-layered cores in an amorphous PEO layer, and (D) a double-layered crystalline PEO lamella with double-layered cores in an amorphous PEO layer. The schematics of these models are shown in Figure 7. From the schematics, models A and B had an extended OMC and models C and D had a folded OMC. The c-axis of PEO 7_2 helices in a monoclinic unit cell was 1.95 nm, and the cross-section area per PEO chain in the crystals was 0.214 nm^2.[42] Since the crystallinity determined by DSC was 80 wt %, each PEO-2K arm had 36.5 repeating units in the crystalline region and 9 repeating units in the amorphous region. It was also possible that three arms of a core were crystalline while one was amorphous. However, this would result in even greater difference in the interfacial areas of the PEO arms and the cores and thus was unlikely to happen. The extended chain length (l_E) for 36.5 repeating units was 10.1 nm. Assuming there were n PEO chains in the cross-section area of one core, the crystalline PEO layer thicknesses for different models in Figure 7 could be obtained (see Table 1). Since the amorphous PEO density was 1.124 g/cm^3,[43] the amorphous PEO volume per core (1584 g/mol) was 2.34 nm^3. Therefore, the total amorphous layer volume (V) was 9.865 nm^3, and the amorphous layer thicknesses for the models in Figure 7 could be estimated, as listed in Table 1. The calculated total lamellar thicknesses (L) were plotted as a function of PEO chains per core for various models in Figure 7. Obviously, models B and D were not possible, since the calculated L (from 21.5 nm for once-folded chain crystals to 43.0 nm for extended chain crystals) was much higher than experimental results. As a result, the single-layered crystalline PEO models A and C might be plausible. Model A had an extended OMC (two arms on each side of the core), while model C had a folded OMC (four arms all on one side of the core). These models were comparable to those observed for two-arm PEO samples.[29,30]

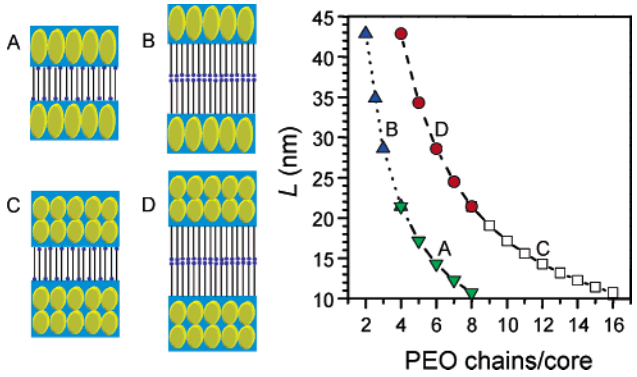

Figure 7. Schematics of possible models and calculated overall lamellar thicknesses (L) as a function of the number of PEO chains per core for these models. Amorphous PEO chains are in light blue without chain details.

Table 1. Crystalline PEO Layer and Amorphous Layer (Including Amorphous Core and Amorphous PEO) Thicknesses as a Function of n PEO Chains per Core for Models A−D in Figure 7

model	n range[a]	crystalline layer thickness (PEO_c)	amorphous layer thickness (Am)
A	4 (E)−8 (1F)	l_E (1.5 − n/8)	9.865/(0.214n)
B	2 (E)−4 (1F)	$2l_E$ (1.5 − n/4)	19.73/(0.214n)
C	8 (E)−16 (1F)	l_E (1.5 − n/16)	9.865/(0.214n) × 2
D	4 (E)−8 (1F)	$2l_E$ (1.5 − n/8)	19.73/(0.214n) × 2

[a] E represents extended chain crystals, and 1F represents once-folded chain crystals.

To evaluate which model is reasonable, L values calculated from the results in Figure 6 are plotted as a function of T_c in parts A and B of Figure 8 for models A and C, respectively. At low T_cs, the increase of L was slow, while it became rapid above 20 °C and nearly leveled off after 40 °C. An increase in L suggested that the crystalline PEO lamellar thickness increased with the T_c, and the amorphous layer (both amorphous PEO and the cores) also had to stretch accordingly. This phenomenon was attributed to the once-folded to extended chain transformation in the PEO-2K crystals with increasing T_c. Assuming that the number of PEO

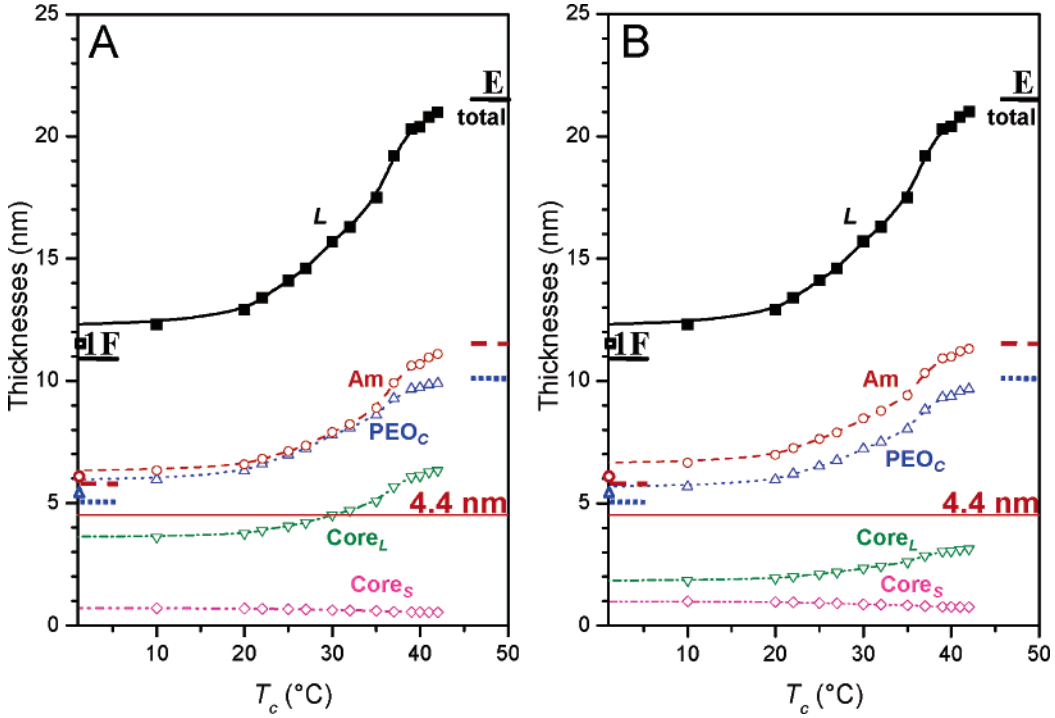

Figure 8. Experimental overall *d*-spacing (L) and calculated thicknesses of amorphous (Am which includes amorphous PEO and cores) and crystalline (PEO_c) layers, and long ($core_L$) and short ($core_S$) axes of the cores as functions of T_c; (A) for model A and (B) for model C. The data for the ASM quenched into liquid nitrogen are shown as open symbols on the coordinate. Thicknesses for once-folded and extended chain crystals are indicated as short bars at low and high T_cs with different colors, respectively.

chains per core was n, L could be calculated as the following for models A and C (see Table 1):

$$\text{model A: } L = 10.1\left(1.5 - \frac{n}{8}\right) + \frac{46.1}{n} \quad (1)$$

$$\text{model C: } L = 10.1\left(1.5 - \frac{n}{16}\right) + \frac{92.2}{n} \quad (2)$$

where L was in nanometers. The first term was the crystalline layer thickness, while the second term was the amorphous layer thickness, including both amorphous PEO and the core. Considering that the cores had an ellipsoidal shape (see discussion below), the short ($core_S$) and the long ($core_L$) axes of the ellipsoid cores could be estimated as

$$\text{core}_S = \sqrt{0.214n/\pi} \quad (3)$$

$$\text{core}_L = \frac{3}{4}V/(0.214n) \quad (4)$$

where V is the volume of the core.

Using these equations and experimental L values, the amorphous and crystalline layer thicknesses and the ellipsoidal core long axes and short axes are plotted in parts A and B of Figure 8 for models A and C, respectively. Comparing the experimental L values with the calculated L, amorphous and crystalline layer thicknesses for once-folded and extended chain crystals (short horizontal bars near the left and right axes in Figure 8), a transition from once-folded to extended chain conformation was clearly seen as the T_c increased. For example, when the ASM was quenched into LN_2, the PEO crystal thickness was 5.4 nm, which was close to the once-folded chain length of 5.0 nm. When the ASM crystallized isothermally at 42 °C, the PEO crystal thickness was 9.7 nm (model C) to 9.9 nm (model A), which was close to the extended chain length of 10.1 nm. At intermediate T_cs, fractionally folded conformations had to be adopted. Obviously, this transition with increasing the T_c was a gradual transition. Generally, nonintegral folds involved both chain ends of a linear chain in the crystal, and the transition from a nonintegral fold to integral folds took place through the cooperative motions of the chain and its ends.[9,10] However, this was not the case for the PEO arms in the ASM sample, which had only one free chain end and the other being attached to the core. It was possible that the fractional folds could involve ciliated chain ends at the crystal surfaces.[44,45] Detailed molecular models for these fractional folds needed future investigation.

The major difference between models A and C was the $core_L$ values, as shown in Figure 8. Since the extended OMC in model A had fewer arms per cross-sectional area of a core (e.g., four arms per core area in extended chain conformation) than the folded OMC in model C (e.g., eight arms per core area in extended chain conformation), the cores in model A had to be much more stretched than in model C (see Figure 8). We noted that the physical length of the core with an extended chain conformation was ca. 4.4 nm as estimated from the molecular model in Scheme 1 using Chem3D (CambridgeSoft, Cambridge, MA). For T_c above 30 °C the calculated $core_L$ for model A was even higher than 4.4 nm and thus was not possible. For model C, the $core_L$ was smaller than 3.3 nm at all the T_cs. Although the $core_L$ was lower than 4.4 nm below 30 °C, the cores in model A were still more stretched than those in model C. Therefore, model C having a folded OMC was plausible, where double-layered cores were packed side by side with four PEO arms of the core all on one side of the core.

The individual layer thicknesses for the PEO crystalline lamella and amorphous layer (including both

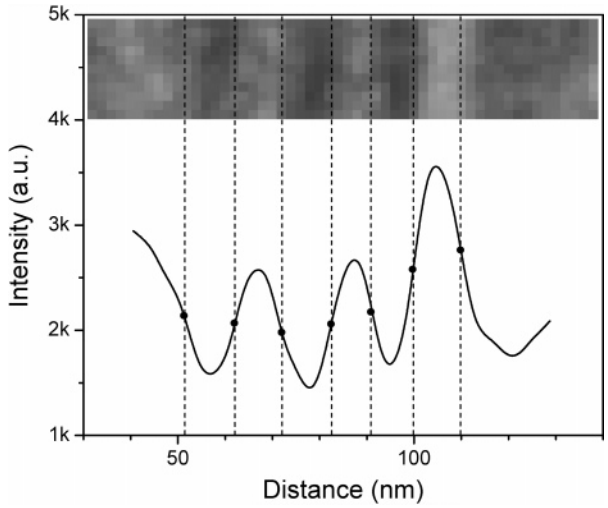

Figure 9. Slice intensity profile of the inset TEM image showing the periodicity of the lamellar structure.

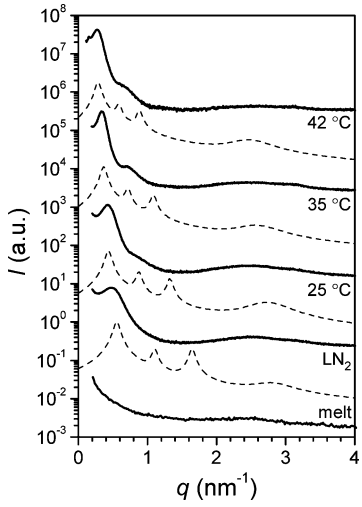

Figure 10. SAXS profiles in the melt and at different T_cs with a short sample-to-detector distance. The dashed curves are calculated structural factors based on the models in Figure 11.

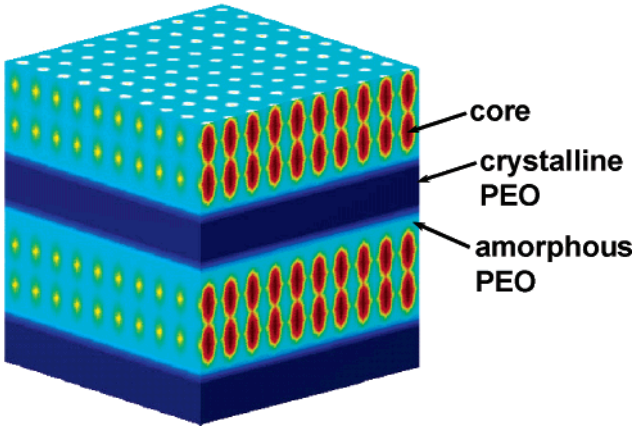

Figure 11. A snapshot of a 64 × 64 × 64 lattice with ellipsoid sizes of $\text{core}_S = 2$ and $\text{core}_L = 4$. For visualization, the densities of crystalline layers, amorphous PEO, and ellipsoids are chosen as 0.15, 0.4, and 0.9.

amorphous cores and PEO) were further confirmed by TEM image analysis. The sample was isothermally crystallized at 40 °C, and the result is shown in Figure 9. From the intensity scan of a stripe in the TEM micrograph (see the inset), individual layer thicknesses could be obtained. Because the staining time was short (10 min), the boundary was diffuse and sinusoidal profile was obtained. Here, we used the inflection points to define the interfacial boundary. From this analysis, the average thicknesses for the dark and bright layers were 9.8 and 9.5 nm, respectively. If RuO_4 stained only the PEO blocks (both amorphous and crystalline PEO), the black and bright layers should be 13.7 and 6.3 nm, since the amorphous PEO layer thickness was ~2.7 nm. Obviously, this was different from what we observed. On the contrary, if RuO_4 stained the amorphous layers (both amorphous PEO and cores), the dark and bright layer thicknesses should be 11.0 and 9.0 nm (see Figure 8B for T_c = 40 °C). Our TEM result was close to the latter case, and thus RuO_4 stained the amorphous layers. Meanwhile, it also proved the validity of our calculations in Figure 8.

It was observed that crystallization rate was closely related to the kinetically controlled chain-folding in the ASM sample. For example, at low T_cs, the crystallization rate was fast (e.g., within 2 min at 10 °C). The cores might not have time for large deformations, and thus the PEO-2K arms had to crystallize into folded-chain conformation. Note that the glass transition temperature (T_g) of the core should be below 10 °C [e.g., the T_g for poly(vinyl dodecanoate), PV-12, was −72 °C[46]]. At high T_cs, the crystallization rate was very slow (a week at 42 °C). Since the cores had enough time for a large deformation (the aspect ratio of $\text{core}_L/\text{core}_S$ = 4.1 at 42 °C), the PEO-2K arms crystallized into the equilibrium extended chain conformation.

Packing of Cores Studied by Computer Simulation of SAXS Intensity. When the SAXS experiments were carried out at a short sample-to-detector distance, the scattering from the lipophilic cores could be observed, as shown in Figure 10. In the melt and solid states at all T_cs, a broad peak centered at 2.5−2.7 nm^{-1} (d-spacing of 2.5 nm) was seen, which was attributed to the structure factor from the cores in the ASM. This also proved our earlier estimation of a core diameter of 2.4 nm. The broad peak in the melt (or correlation-hole scattering) indicated the existence of disordered morphology in the ASM. Judging from the full width (~1.2 nm^{-1}) of these broad peaks in the solid state, the correlation length among neighboring cores must be short (or liquidlike). A striking feature of the core scatterings was that the peak positions were similar for all T_cs, and in the melt, no matter how much the cores became elongated at high T_cs. To explain this phenomenon, the SAXS intensity at different T_cs was calculated by computing the structure factors of a three-dimensional (3D) model based on the model in Figure 11. The 3D model was built using the calculated values for the amorphous (including the amorphous PEO and the cores) and crystalline layers and long and short axes of the cores in Figure 8B. Note that in this model each phase had a uniform density with no molecular details. The results are shown in Figure 10 as the dashed-line curves. It was seen that the first and second lamellar reflections agreed well with the experimental results. The broad peak centered in the range 2.4−2.8 nm^{-1} originates from the average distance between neighboring ellipsoids. These broad reflections also generally agreed with the experimental SAXS results, except for a slight mismatch at low T_cs. From these results, the shape of the cores did not substantially alter their

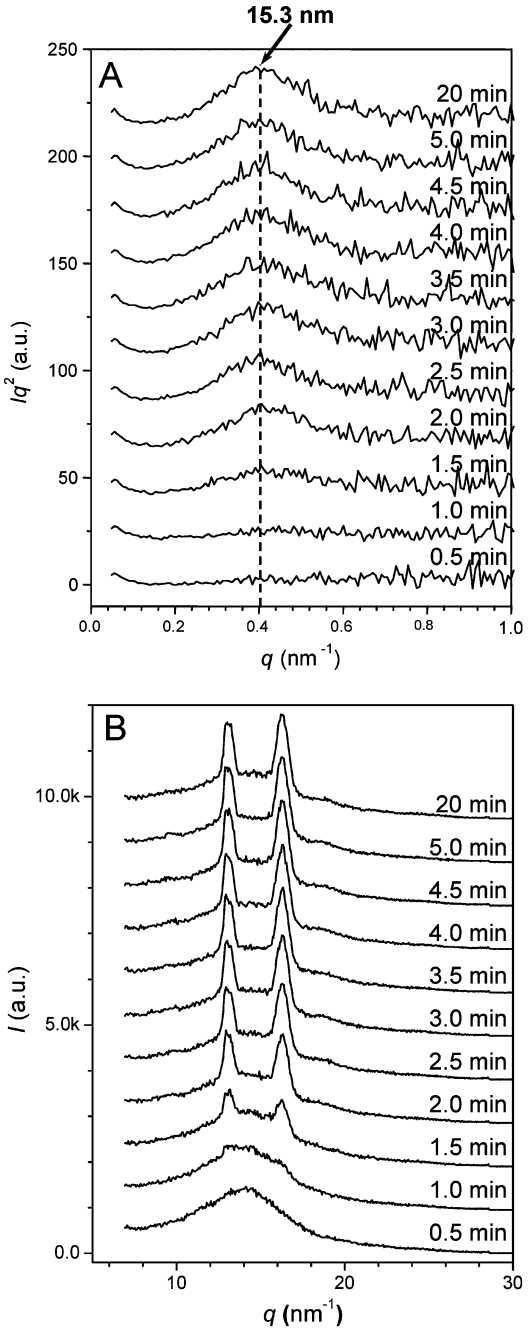

Figure 12. (A) SAXS and (B) WAXD profiles for the ASM isothermally crystallized at 27 °C at different times.

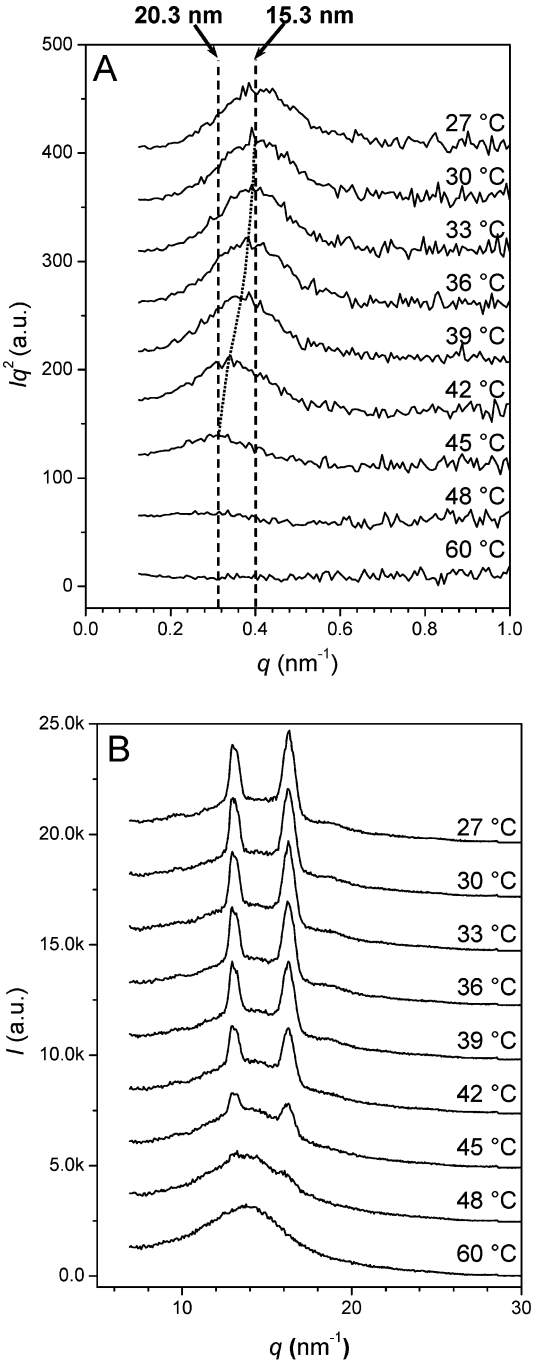

Figure 13. (A) SAXS and (B) WAXD profiles for the melting process after the ASM fully crystallized at 27 °C.

scattering profiles around $q = 2.5$ nm^{-1} as long as the packing of the cores was liquidlike.

Isothermal Crystallization and Subsequent Melting Studied by Simultaneous SAXS and WAXD. The phase structure development in the ASM was studied by time-resolved simultaneous SAXS and WAXD techniques. The 1D SAXS and WAXD results of an isothermal crystallization process at 27 °C are shown in parts A and B of Figure 12, respectively. The broad lamellar reflection appeared at 1.5 min, with an average *d*-spacing of 15.3 nm. This lamellar morphology was a result of PEO crystallization as evidenced in the WAXD profile at 1.5 min in Figure 12B. With increasing the crystallization time, the lamellar reflection increased its intensity but remained at a constant position throughout the whole crystallization process. Based on the interpretation in Figure 8B, a *d*-spacing of 15.3 nm indicated a fractional chain-folding of the PEO arms. The invariant lamellar thickness throughout the crystallization suggested a consistent metastability of the fractionally folded crystals at this particular temperature. Note that this was different from the nonintegrally folded crystals in PEO oligomers during an isothermal crystallization, which transformed into integrally folded crystals through thinning and/or thickening processes.[10]

The metastability of the fractionally folded crystals was further studied at elevated temperatures during a melting process at a heating rate of 1 °C/min. In Figure 13A, when the temperature increased to 33 °C, the lamellar reflection started to shift to lower *q* values, indicative of a thickening process of the fractionally folded lamellar crystals. When the temperature increased to 39 °C, the PEO crystals began to melt, as

shown by a slight crystallinity drop in the WAXD profiles in Figure 13B. Meanwhile, the lamellar *d*-spacing was 17.1 nm. Finally, at 45 °C the remaining lamellar crystals had an overall thickness of 20.3 nm, which was close to an extended chain conformation. This thickening process must involve cooperative motions of the PEO arms in the crystals. From these results, it was concluded that the extended chain conformation could be obtained faster by annealing at elevated temperatures through a melt-reorganization mechanism, rather than isothermal crystallization from the quiescent melt.

Conclusions

In the ASM, we observed substantial *d*-spacing increases with increasing the T_c, suggesting gradual transitions from once-folded to fractionally folded and finally to extended chain crystals. The once-folded and fractionally folded crystals were formed kinetically, while extended chain crystals were the equilibrium structure for ASM sample. The extended chain conformation could be obtained faster by annealing at elevated temperatures rather than isothermal crystallization from the quiescent melt. On the basis of the SAXS, TEM, and computer simulation results, the lamellae contained an interdigitated, single-layered PEO crystal and an amorphous layer consisted of a double-layered lipophilic core and amorphous PEO. A folded rather than an extended OMC of the ASM was deduced in the solid state.

Acknowledgment. This work was supported by ACS PRF 41918-G7 (L.Z.), NSF CAREER awards, DMR-0348724 (L.Z.), BES-9983272 (K.E.U.), and DMR-0094290 (M.U.). The synchrotron SAXS experiments were carried out in the National Synchrotron Light Source, Brookhaven National Laboratory, supported by the DOE (Grant DE-FG02-99ER 45760). L.Z. also thanks helpful discussions with Prof. Alexei P. Sokolov and Dr. Yifu Ding at the University of Akron.

References and Notes

(1) Lehn, J.-M. *Supramolecular Chemistry—Concepts and Perspectives*; VCH: Weinheim, 1995.
(2) Hamley, I. W. *Adv. Polym. Sci.* **1999**, *148*, 113.
(3) Zhu, L.; Chen, Y.; Zhang, A.; Calhoun, B. H.; Chun, M.; Quirk, R. P.; Cheng, S. Z. D.; Hsiao, B. S.; Yeh, F.; Hashimoto, T. *Phys. Rev. B* **1999**, *60*, 10022.
(4) Wunderlich, B. *Macromolecular Physics;* Academic Press: New York, 1973; Vol. 1.
(5) Davis-Searles, P. R.; Saunders, A. J.; Erie, D. A.; Winzor, D. J.; Pielak, G. J. *Annu. Rev. Biophys. Biomol. Struct*. **2001**, *30*, 271.
(6) Ungar, G.; Zeng, X.-B. *Chem. Rev.* **2001**, *101*, 4157.
(7) Ungar, G.; Stejny, J.; Keller, A.; Bidd, I.; Whiting, M. C. *Science* **1985**, *229*, 386.
(8) Kovacs, A. J.; Gonthier, A.; Straupe, C. *J. Polym. Sci., Polym. Symp.* **1975**, *50*, 283.
(9) Ungar, G.; Keller, A. *Polymer* **1986**, *27*, 1835.
(10) Cheng, S. Z. D.; Zhang, A.; Chen, J. H.; Heberer, D. P. *J. Polym. Sci., Part B: Polym. Phys.* **1991**, *29*, 287.
(11) Muthukumar, M.; Ober, C. K.; Thomas, E. L. *Science* **1997**, *277*, 1225.
(12) Chen, Y.; Baker, G. L.; Ding, Y.; Rabolt, J. F. *J. Am. Chem. Soc.* **1999**, *121*, 6962.
(13) DiMarzio, E. A.; Guttman, C. M.; Hoffman, J. D. *Macromolecules* **1980**, *13*, 1194.
(14) Whitmore, M. D.; Noolandi, J. *Macromolecules* **1988**, *21*, 1482.
(15) Vilgis, T. A.; Halperin, A. *Macromolecules* **1991**, *24*, 2090.
(16) Douzinas, K. C.; Cohen, R. E.; Halasa, A. F. *Macromolecules* **1991**, *24*, 4457.
(17) Unger, R.; Beyer, D.; Donth, E. *Polymer* **1991**, *32*, 3305.
(18) Rangarajan, P.; Register, R. A.; Fetter, L. J. *Macromolecules* **1993**, *26*, 4640.
(19) Nojima, S.; Yamamoto, S.; Ashida, T. *Polym. J.* **1995**, *27*, 673.
(20) Lee, L.-B. W.; Register, R. A. *Macromolecules* **2004**, *37*, 7278.
(21) Ashman, P. C.; Booth, C. *Polymer* **1975**, *16*, 889.
(22) Booth, C.; Pickles, C. J. *J. Polym. Sci., Polym. Phys.* **1973**, *11*, 259.
(23) Viras, F.; Luo, Y.-Z.; Viras, K.; Mobbs, R. H.; King, T. A.; Booth, C. *Makromol. Chem.* **1988**, *189*, 459.
(24) Yang, Y.-W.; Tanodekaew, S.; Mai, S.-M.; Booth, C.; Ryan, A. J.; Bras, W.; Viras, K. *Macromolecules* **1995**, *28*, 6029.
(25) Ryan, A. J.; Fairclough, J. P. A.; Hamley, I. W.; Mai, S.-M.; Booth, C. *Macromolecules* **1997**, *30*, 1723.
(26) Mai, S.-M.; Fairclough, J. P. A.; Viras, K.; Gorry, P. A.; Hamley, I. W.; Ryan, A. J.; Booth, C. *Macromolecules* **1997**, *30*, 8392.
(27) Hong, S.; Yang, L.; MacKnight, W. J.; Gido, S. P. *Macromolecules* **2001**, *34*, 7009.
(28) Opitz, R.; Lambreva, D. M.; de Jeu, W. H. *Macromolecules* **2002**, *35*, 6930.
(29) Lee, S.-W.; Chen, E.-Q.; Zhang, A.; Yoon, Y.; Moon, B.-S.; Lee, S.; Harris, F. W.; Cheng, S. Z. D.; von Meerwall, E. D.; Hsiao, B. S.; Verma, R.; Lando, J. B. *Macromolecules* **1996**, *29*, 8816.
(30) Chen, E.-Q.; Lee, S.-W.; Zhang, A.; Moon, B.-S.; Honigfort, P. S.; Mann, I.; Lin, H.-M.; Harris, F. W.; Cheng, S. Z. D.; Hsiao, B. S.; Yeh, F. *Polymer* **1999**, *40*, 4543.
(31) Maclaine, J. Q. G.; Ashman, P. C.; Booth, C. *Polymer* **1976**, *17*, 109.
(32) Chen, E.-Q.; Lee, S.-W.; Zhang, A.; Moon, B.-S.; Mann, I.; Harris, F. W.; Cheng, S. Z. D.; Hsiao, B. S.; Yeh, F.; von Meerwall, E. D.; Grubb, D. T. *Macromolecules* **1999**, *32*, 4784.
(33) Galin, J.-C.; Spegt, P. A.; Suzuki, S.; Skoulios, A. E. *Makromol. Chem.* **1974**, *175*, 991.
(34) Flory, P. J.; Vrij, A. *J. Am. Chem. Soc.* **1963**, *85*, 3548.
(35) Tian, L.; Yam, L.; Zhou, N.; Tat, H.; Uhrich, K. E. *Macromolecules* **2004**, *37*, 538.
(36) Liu, H.; Jiang, A.; Guo, J.; Uhrich, K. E. *J. Polym. Sci., Part A: Polym. Chem.* **1999**, *37*, 703.
(37) Tian, L.; Uhrich, K. E., manuscript in preparation.
(38) Trent, J. S.; Scheinbeim, J. I.; Couchman, P. R. *Macromolecules* **1983**, *16*, 589.
(39) Buckley, C. P.; Kovacs, A. J. *Prog. Colloid Polym. Sci.* **1975**, *58*, 44.
(40) Sun, L.; Liu, Y.; Zhu, L.; Avila-Orta, C. A.; Hsiao, B. S. *Polymer* **2004**, *45*, 8181.
(41) Zhu, L.; Cheng, S. Z. D.; Calhoun, B. H.; Ge, Q.; Quirk, R. P.; Thomas, E. L.; Hsiao, B. S.; Yeh, F.; Lotz, B. *J. Am. Chem. Soc.* **2000**, *122*, 5957.
(42) Tadokoro, H. *Structure of Crystalline Polymers*; John Wiley & Sons: New York, 1979.
(43) Zhu, L.; Cheng, S. Z. D.; Calhoun, B. H.; Ge, Q.; Quirk, R. P.; Thomas, E. L.; Hsiao, B. S.; Yeh, F.; Lotz, B. *Polymer* **2001**, *42*, 5829.
(44) Hoffman, J. D. *Polymer* **1991**, *32*, 2828.
(45) Hoffman, J. D.; Miller, R. L. *Polymer* **1997**, *38*, 3151.
(46) Plate, N. A., Shibaev, V. P., Ed.; *Comb-Shaped Polymers and Liquid Crystals*; Plenum Press: New York, 1987; p 129.

MA050983Q